Growth and Transport Properties of [Rare Earth]TiO3/SrTiO3 Interfaces

Lebedev, N.

1

Literature Review

1

1.1. Introduction

The two-dimensional electron gas, or rather liquid (2DEL), at oxide interfaces and based on $SrTiO_3$ (STO) has a rich phenomenology. A review of all the phenomena in this system is beyond the scope of the present work. This chapter is constrained to the most relevant results for this thesis. Moreover, the careful reader will notice that some parts of this chapter duplicate information presented in other chapters. That has been done intentionally to keep each chapter self-contained. This chapter will start with a description of the STO band structure, the formation of the 2DEL at the oxide interfaces, the role of Spin-Orbit Coupling (SOC), the occurrence of multiband transport at the interface, and the effects of a back gate voltage. Also superconductivity and magnetism occurring in the 2DEL at oxide interfaces will be introduced. Special attention will be given to the Anomalous Hall Effect (AHE) and its observation at oxide interfaces. The end of the chapter will be an overview of bulk and thin film properties of (RE)TiO_3 (Re=La, Gd, Eu, $Eu_{1-x}La_x$), which are the building blocks for the interfaces to come.

1.2. Conducting oxide interfaces

1.2.1. Formation of the two-dimensional electron liquid at oxide interfaces

In a simple picture semiconductors or insulators have one important quality which make them different from metals, namely the presence of a band gap [9]. In direct- and indirect-gap semiconductors, the Fermi level lies above a filled valence band, but below an empty conduction band, and it requires (thermal) excitations of the charge carriers to invoke conduction. However, semiconductors can be doped by atoms with different valence, thereby changing the position of the Fermi level and leading to conductivity. These atoms can be evenly distributed over whole crystal or they can be incorporated in a certain atomically thin sheet. That is called a δ-doping. Unintentional doping can also occur due to vacancies in crystal structures [9]. By combining semiconducting materials with different band gaps, so-called quantum wells (QWs) can be created. Consider the spatial variation of the conduction band edge when a very thin layer of GaAs with a smaller band gap is sandwiched between layers of AlGaAs with a larger band gap, as shown in Fig. 1.1a. Because of the confinement, electron levels are formed which are quantized in the stacking direction (the z-direction), but free in the plane directions. This is why

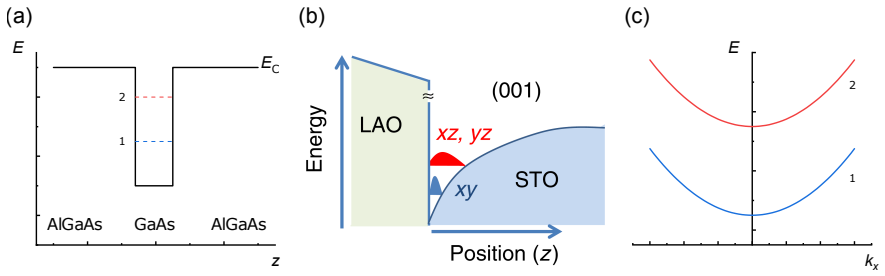

Figure 1.1: (a) The conduction band edge variation of AlGaAs/GaAs/AlGaAs heterostructure forming a quantum well. (b) Quantum well formation at a single (oxide) interface. The figure is adopted from Ref. [12]. Copyright 2015 by Springer Nature. (c) The lowest two parabolic bands in a quantum well heterostructure.

the electron system is two-dimensional. Similar confinement can be created at a single interface, using different degrees of doping and the ensuing phenomenon of band bending. A schematic example is given in Fig. 1.1b. The QW shape is triangular rather than rectangular, but the principle is the same. This is the situation encountered in $LaAlO_3/SrTiO_3$ (LAO/STO). The in-plane energy dispersion of the quantized levels can be described by a set of parabolic bands (Fig. 1.1c) where the first two levels are shown. If the material consists of heavy atoms with a large nuclear charge, there may be non-negligible spin-orbit coupling (SOC), which lifts spin degeneracy of the bands. Moreover, a quantum well heterostructure lacks spatial inversion symmetry and an additional contribution to the SOC arises, which is called the Rashba effect [10, 11]. One point of interest, in particular for the single-heterojunction QW, is that band occupancy and carrier concentration can be tuned by applying an electric field through a metal contact on one of the semiconductors (the gate). This electrode and the 2DEG can then be seen as a parallel plate capacitor, so the carrier concentration can be changed by applying a gate voltage.

Now we turn to the interface between transition oxide insulators, where QWs and a 2DEL form as well. The most studied oxide interface is between the non-magnetic band insulators LAO and STO [2]. LAO has a band gap of about 5.6 eV [13], whereas STO has a band gap around 3.2 eV [14, 15]. Both are perovskites of type ABO_3 and have a pseudocubic crystal structure. LAO shows a small rhombohedral distortion, STO is cubic at room temperature and undergoes a structural transition to tetragonal below 105 K [16, 17]. LAO is a polar material. It consists of a stacking of LaO and AlO_2 layers, which means a stacking of sheets with -1 and +1 electron charges. STO is non-polar and consists of a stacking of SrO and TiO_2, which means a stacking of charge-neutral layers. A charge discontinuity therefore

occurs at the interface, which is often referred to as the polar catastrophe, From simple electrostatics, the discontinuity can be avoided by the transfer of half an electron charge ($e/2$) per unit cell (u.c.) from the LAO surface to the LAO/STO interface. The first proposed explanation for the formation of the 2DEL was based on such simple charge transfer [18, 19]. Supporting this model is the fact that a minimum critical thickness for the LAO layer grown on top of an STO substrate of 4 u.c. is needed before the 2DEL is formed [20]. However, various experiments were at odds with this explanation, and other scenario's were proposed. One is the development of a critical density of oxygen vacancies at the surface of the LAO layer, which leads to a charge transfer of $2e$ per vacancy to the interface [19, 21]. Also, La/Sr intermixing [22] and oxygen vacancies formed in the STO [23, 24] can introduce conductivity at the STO surface, and the last mechanism appears especially important in 2DELs formed at the interface between and STO and amorphous oxides [25, 26]. One important remark should be made here. Almost invariably, a single crystal substrate is used for the STO side of the interface, and only films grown on the TiO_2-terminated surface of STO exhibit an (n-type) conductivity [2, 18]. An interface created by the growth of LAO on a SrO-terminated surface was expected to be a p-type but turned out to be insulating [18]. This has lent more credence to the indications that oxygen vacancies in the top TiO_2 surface, probably even formed during the growth of LAO, are important for the 2DEL formation.

Following up on the bandstructure of the 2DEL, the n-type doping will induce electrons in $3d$ orbitals of the Ti at the interface. In free atom, the Ti orbitals are ten-fold degenerate, but in the bulk STO the six nearest oxygen atoms produce a cubic crystal field, which leads to a t_{2g} triplet (d_{xy}, d_{yz}, d_{xz}) and e_g doublet (d_{z^2}, $d_{x^2-y^2}$) [15, 29]. Since the t_{2g} triplet lies 2 eV lower than the e_g doublet, it forms the conduction band minimum [29–31], and further consideration is limited to these states. The corresponding bulk band structure is shown in the Fig. 1.2a. The SOC in the STO leads to the splitting of the triplet state, which is six times degenerate, into four times and two times degenerate levels with a splitting around ≈ 29 meV as determined from theoretical calculations [27, 28, 32](Fig. 1.2b). Below 105 K STO undergoes a cubic to tetragonal transition [16, 17], which further splits the triplet into two states with splitting $\approx 2-3$ meV and breaks the symmetry along k_x and k_z [15, 27, 33, 34](Fig. 1.2c). However, it is hard to experimentally determine a value of the splitting due to the SOC in the tetragonal phase [30]. At the LAO/STO (001) interface inversion symmetry is broken. This shifts the in-plane d_{xy} orbitals below the out-of-plane $d_{xz/yz}$ ones, corresponding with a splitting between them of 50 meV as determined by X-Ray Linear Dichroism Measurements (XMCD) [33]. The SOC hybridizes the orbitals [28, 34]. The above picture of the interface states essentially represents two bands, one of them with a light effective mass in the in-plane direction and a heavy mass in the out-of-plane direction,

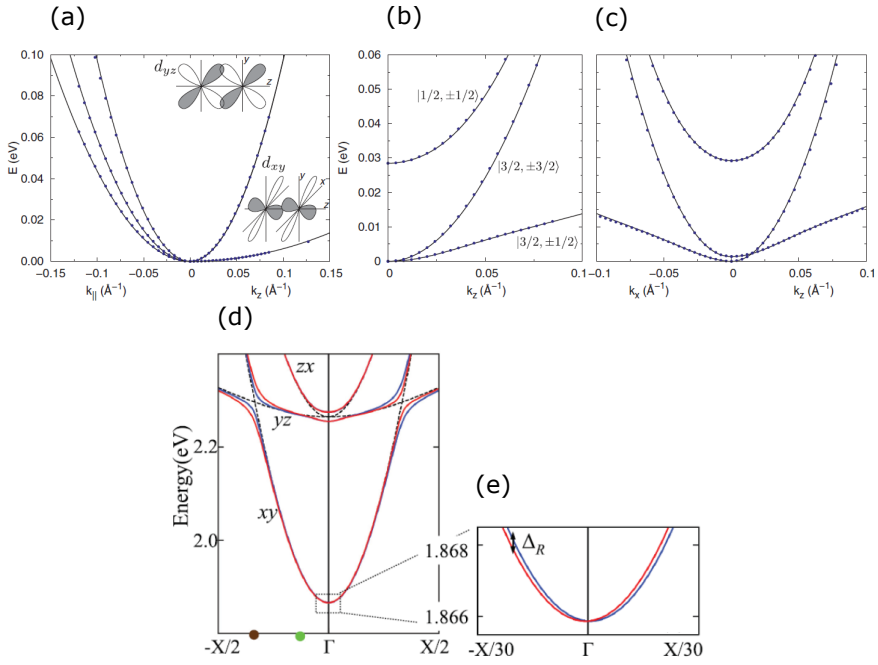

Figure 1.2: The DFT calculation of the STO band structures in (a) cubic crystal lattice without the SOC, (b) cubic crystal lattice with the SOC (the bands are shifted in such way that the bottom correspond to the zero energy) and (c) tetragonal crystal structure with the SOC. The figures a, b, c are reprinted from Ref. [27]. Copyright 2013 by the American Physical Society. (d) The tight binding calculations of the band structure of the LAO/STO interface and (e) zoom at the bottom of the d_{xy} band. The blue and red colors correspond to different spins. The figures d and e are reprinted from Ref. [28]. Copyright 2013 by the American Physical Society.

whereas the second band has a heavier effective mass in-plane than out-of-plane. The different band curvature together with the spitting leads to the formation of avoided band crossing [27, 32] as can be seen on the Fig. 1.2d. Furthermore, the consequence of broken inversion symmetry is Rashba-like spin splitting [5, 32], which produces two characteristic features, namely small spin splitting at the bottom d_{xy} band (Fig. 1.2e) and stronger splitting near the avoided band crossing between the d_{xy} and $d_{xz/yz}$ bands [27, 28, 32, 35] (Fig. 1.2d). Clearly, the Ti-3d-derived band structure of the quantum well states is far from trivial, and leads to many intriguing phenomena. Several will be discussed later, but an important one is that the system can be switched from one-band (the d_{xy} band) to two-band behavior (filling the $d_{xz/yz}$ band) by moving the Fermi energy through the anticrossing point with a gate voltage. Since this also entails a change in Fermi surface topology, this

point (in voltage) is called a Lifshitz point [32, 35, 36]. Crossing the Lifshitz point leads to sometimes subtle changes in transport properties, which requires careful analysis. The most clear transport signature of such a transition is the change from a linear to a non-linear Hall effect [36, 37].

The main signatures of the absence or presence of SOC in magnetotransport experiments, specifically in magnetoresistance (*MR*), are weak localization (WL) and weak antilocalization (WAL). Both phenomena have been extensively studied in semiconducting materials and require special attention since, as mentioned in the introduction, controlling the amount of spin orbit coupling can be useful in devices. WL occurs in a disordered metallic system, both with no or little SOC and gives a negative correction to the conductivity due to quantum interference, which enhances the probability for backscattering [38–40]. WAL arises when the SOC is present, because spin relaxation becomes important in the interference effects. Strong SOC adds an additional phase to the interference, leading to a positive instead of a negative correction [39, 41–43]. Both WL and WAL have been observed experimentally in LAO/STO [5, 44, 45]. Due to the fact that the Rashba coupling constant can be tuned directly by changing electric field by applying the gate voltage [5, 46], or by changing the carrier concentration [46], the *MR* can also show a transition from WAL to WL [4, 5]. Early studies of the gate dependence of the Rashba coupling provided contradicting results. Ref. [5, 12] reported an increase of the Rashba coupling constant with increasing of the gate voltage, but Ref. [47] observed the opposite trend. Later reports found that the Rashba coupling peaks near the Lifshitz point [46, 48], which seems to be in agreement with spin-to-charge conversion experiments [49]. An unresolved subtlety with respect to the effects of SOC is the question of its k-dependence. In bulk materials with inversion symmetry, the k-dependence is linear. Without inversion symmetry, a cubic k-dependence becomes possible, and was reported by in Refs. [48, 50], whereas Ref. [46] argued that the dominant SOC contribution is k-linear.

Next we come to the effects of applying a gate voltage in oxide heterostructures. Because both STO and LAO are insulating, they can be used as a barrier for applying a gate voltage. This allows utilizing various geometries of gate electrodes. In the present work, a back gate geometry has been used, where the STO substrate has been used as the dielectric layer. In spite of the large thickness of STO substrate, this geometry is relatively effective due to large permittivity of STO at low temperatures. The back gate voltage controls not only the carrier concentration, but also the width of the (triangular) quantum well, and therefore strongly affects the amount of disorder sampled [51]. Generally, a decrease of the back gate voltage leads to narrower potential well and lower mobility [52, 53]. One of the most prominent effects of applying a back gate voltage to STO-based heterostructures

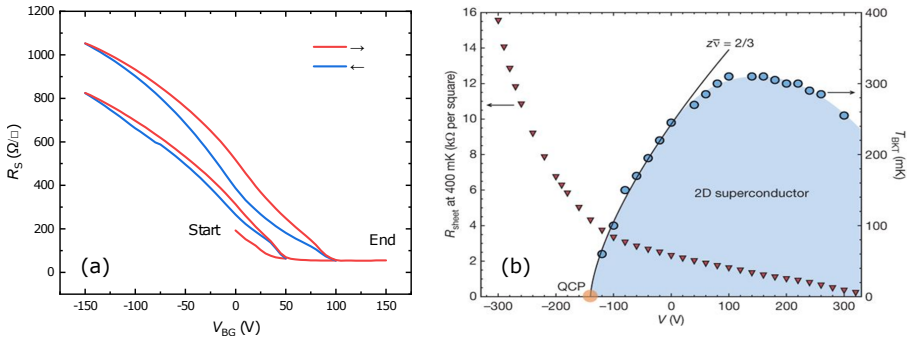

Figure 1.3: (a) The dependence of the sheet resistance R_S on the backgate voltage for a LAO/STO sample. The voltage was swept in the following sequence: from 0 to 50 V, from 50 V to −150 V, from −150 to 100 V, from 100 V to −150 V, from −150 V to 150 V. (b) The dependence of R_S and of the critical temperature T_c on the gate voltage for a LAO/STO sample at 400 mK. The figure is adopted from Ref. [4]. Copyright 2008 by Springer Nature

is hysteresis due to charge trapping [52, 54, 55]. This effect is observed when, at the first time after cooldown, a significant positive voltage is applied to the heterostructures, i.e. a voltage that has not been reached in previous voltage sweeps during that particular cooldown. As an example, Fig. 1.3a shows the dependence of the sheet resistance on the applied back gate voltage for a LAO/STO sample measured at 3 K and prepared for this thesis. The first detailed study of this phenomenon was performed by Biscaras *et al.* [54]. They proposed that at the initial cooldown, the Fermi level lies close to the top of the quantum well, and after filling to a certain threshold, electrons are able to escape irreversibly into the STO substrate, where they are trapped in defects. Recently, Ref. [55] put forward an alternative explanation based on the formation of in-gap trapping states due to clustering of oxygen vacancies. For more details on experimental aspects of back gate experiments see Section 2.3. The strong effect of charge trapping and variation of the disorder together with carrier concentration [52, 53] led to a significant effort to develop top-gating experiments. These experiments utilize the LAO layer as a dielectric insulator and allow to control charge filling with the top gate but do not change the shape of the potential well [37, 53, 56]. The combination of top-and back-gate configurations allows independently, but still simultaneously, to control carrier concentration and disorder [51, 53]. The top gate experiments will not be discussed further.

1.2.2. Superconductivity at oxide interfaces

Gating changes the carrier concentration in the QW, the amount of bands involved, and the strength of SOC, which has consequences for magnetotransport. What has not yet been mentioned is that also cooperative electron phenomena occur at oxide interfaces, in particular superconductivity and magnetism of some kind, plus related effects such as the Kondo effect or the possible coexistence of superconductivity and magnetism. Gate-tunability provides additional control over these phenomena as well. In order to discuss the experiments on superconductivity at the LTO/STO and LAO/GTO/STO interfaces, we first introduce the basic framework of the occurrence of superconductivity at STO-based interfaces.

Being a 2DEL, the LAO/STO interface exhibits a superconducting transition of the so-called Berezinskii-Kosterlitz-Thouless (BKT) type [3, 57]. The BKT transition is a thermodynamic instability in which spontaneoulsy formed vortex-antivortex pairs, bound at low temperatures, dissociate into free vortices at a characteristic temperature, T_{BKT}, which lies below the bulk T_c, and basically only depends on the sheet resistance of the thin fim or 2D metal. The superconducting state is tunable by the gate voltage [4, 52] and has a dome-like critical temperature dependence on the applied voltage (Fig. 1.3b). At the moment, there is no full agreement on the role of the band structure, and in particular the one-band to two-band transition, with respect to the superconducting transition. Ref. [36] reported that the maximum of the dome corresponds to the Lifshitz point, but Refs. [58, 59] argued that superconductivity is triggered by the onset of the occupation of the second band. Ref. [51] found that the dome maximum is correlated with the occupation of the second $3d_{xy}$ subband.

The superconducting state in STO-based structures often exhibits signatures of inhomogeneities such as hysteretic IV curves [60, 61] and multiple steps in the temperature dependence of the resistance close to the transition region [51, 61, 62]. Broadening of the superconducting transition has also been attributed to inhomogeneities [62–64]. Such inhomogeneities can arise due to some phase separation between electron-dense and less dense domains [63, 65]. Another important source of inhomogeneities in STO-based interfaces are the tetragonal domains which appear below the cubic to tetragonal structural transition at 105 K [66–69]. These domains are stable with changing temperature, as long as the sample is not cycled above that temperature [66, 69]. On the other hand, they can be tuned by the back gate voltage [66, 68, 69], and it has also been shown that this domain structure strongly modulates conduction paths [66], and even that the different domains have different transition temperatures [67].

Besides the gate dependence of the critical temperature, Caviglia *et al.* [4] have observed a Superconductor-to-Insulator (SIT) transition near a sheet resistance value of 6.5 kOhm. The physics of this transition is still under debate. There is the 'dirty boson' scenario, which means that the strong disorder causes an electronic phase separation, with isolated superconducting islands in a sea of insulating material even up to localized Cooper pairs [70–72]. There is also a Fermionic scenario, in which Cooper pairs are destroyed by various mechanisms in the insulating phase [71]. A scaling analysis of the behavior of the magnetic field dependence of the sheet resistance around the SI transition in LTO/STO revealed non-universal behavior as function of the gate voltage. A critical exponent product $\nu z = 2/3$ was found in one regime, favoring the Fermionic scenario, but $\nu z = 3/2$ in another, stipulating the dirty boson scenario. At the same time, a similar study on LAO/STO found $\nu z = 7/3$ corresponding to the bosonic scenario [73]. For such critical exponents the insulating phase is in a quantum percolation state, in which Cooper pairs tunnel between localized superconducting islands [72, 73]. Also the complex behavior of *MR* hysteresis across the SIT was interpreted as evidence of such a scenario [74].

1.2.3. Magnetism in oxide interfaces

In spite of the intense investigation of the LAO/STO conducting interface over last 15 years, there is no consensus on the low-temperature magnetic state of the system [19, 75]. Polarized neutron refractometry showed a small number of magnetic moments localized at the interface in multilayer samples [76]. Magnetic torque measurements revealed superparamagnetic behavior of the magnetization in LAO/STO, but were not able to detect a change in low field dependence of the magnetic moment up to 40 K [7] as would have been expected. Scanning SQUID microscopy detected the presence of ferromagnetic patches [6]. Ariando *et al.* [65] have observed diamagnetic, paramagnetic and ferromagnetic contributions in LAO/STO in SQUID magnetometry experiments, which varied with the growth pressure, with both the diamagnetic one and the ferromagnetic one increasing in samples grown at higher pressure. Coey *et al.* [77] investigated a number of STO crystals from different suppliers and found multiple contributions to magnetism: an extrinsic signal related to ferromagnetic impurities from the preparation process and an intrinsic isotropic magnetic signal from the surface. That signal, with saturation behavior and almost absent hysteresis, was observed in a wide range of temperatures. Different possible scenarios have been discussed, but no model was able to provide a full and satisfactory explanation. Moreover, recent scanning SQUID experiments revealed striped magnetic modulation coupled

to the ferroelastic domains in STO based heterostructures [78]. The modulation disappears below 8 K, which was attributed to the establishing of magnetically ordered state.

A number of experiments also indicate coexistence of superconductivity and magnetism in STO-based heterostructures. The magnetic patches detected by the scanning SQUID microscopy [6] and the magnetic order observed by the magnetic torque [7] were found to be present below the superconducting transition. Furthermore, hysteretic *MR* was reported in superconducting LAO/STO [8, 74, 79, 80] and attributed to a signature of coexistence of superconductivity and magnetism. On the other hand, some experiments showed presence of hysteretic *MR* in the milliKelvin range due to magnetocaloric effect [81, 82]. Generally, the picture is one of poor reproducibility [83].

A few theories of magnetism at the LAO/STO interface have been proposed. They can be separated in intrinsic and extrinsic effects [83]. Among the intrinsic mechanisms are localized carriers [84, 85], itinerant ferromagnetism [86, 87] or ferromagnetism arisen from localized electrons and mediated by conduction electrons [88–90]. On the other side, extrinsic mechanisms have been proposed such as Sr vacancies [91], Al vacancies [92], oxygen vacancies [93, 94] and magnetic contamination [77, 83]. On the whole, a systematic study [83] of the LAO/STO interface by various techniques concluded that intrinsic mechanisms for magnetism are unlikely to be the origin of the magnetic effects in LAO/STO.

1.2.4. Kondo-like behavior

One of the first results on LAO/STO signaling the possible presence of magnetic effects in transport was the work by Brinkman *et al.* [95]. Apart from the *MR* hysteresis they found at low temperatures in a particular range of oxygen-growth pressures, in the same range they observed a resistance upturn at low temperatures with saturation at the lowest temperature. They proposed that that can arise due to the Kondo effect, a behavior in agreement with an oxygen vacancy picture of the origin of the magnetism. This Kondo effect is expected to arise due to localized magnetic moments. Ref. [90, 96] argued that the magnetic moments are a small amount of localized Ti $3d_{xy}$ electrons, which can be regarded as impurities. The d_{xy} bands lie in the plane of interface, and mobile $3d_{xy}$ electrons couple antiferromagnetically to magnetic moments. In contrast, the $d_{xz/yz}$ band is perpendicular to the interface plane, and $3d_{xz/yz}$ electrons couple ferromagnetically with the magnetic moments. Therefore, tuning the system through the Lifshitz point should also change a Kondo-like state to a ferromagnetic state. According to the

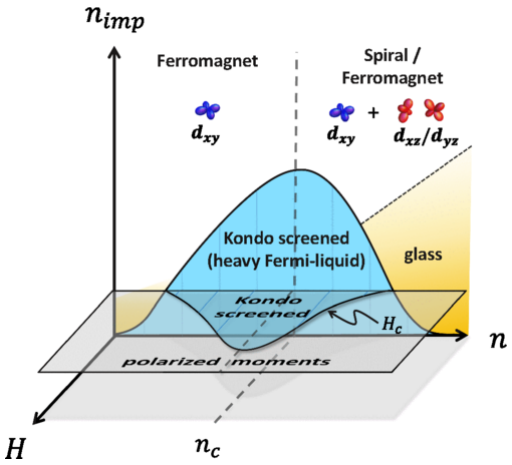

Figure 1.4: (a) The phase diagram for magnetism at the LAO/STO interface proposed by Ruhman *et al.* n is the electron density, n_{imp} is the density of local magnetic moment, H is the in-plane magnetic field, and n_c is the critical density above which the second band is filled. The figure is reprinted from Ref. [90]. Copyright 2014 by American Physical Society.

theory proposed by Ruhman *et al.*, the indirect RKKY exchange interaction will be competing with Kondo screening, and therefore, the dominant behavior would depend not only on the carrier concentration n but also on the concentration of 'impurity' magnetic moments n_{imp}. From this theory, a magnetic phase diagram for these two values will have a dome-like shape with a maximum at the Lifshitz point, as shown in Fig. 1.4. Kondo screening will disappear at very low electron densities deep inside an insulating phase and at very high electron densities deep inside of the two-band regime [90]. Such a model might explain specific features in magnetotransport data, in particular a drop of in-plane magnetoresistance. Below a certain critical in-plane field, the magnetic moments are Kondo-screened, and the unitary scattering leads to high resistance. Above that field, the Kondo singlet breaks up, the moments become polarized, and the resistance decreases [90, 96, 97]. The critical field will also have a-dome like density dependence according to [90] with a maximum around Lifshitz point (see Fig. 1.4).

However, Diez *et al.* [98] found that behavior of the negative in-plane *MR* persists up to 20 K, which does not fit in the framework of the (temperature dependent) Kondo picture. Instead, they described it within single-particle Boltzmann transport theory, showing that the large negative *MR* can be produced by the SOC, the anisotropy of the Fermi surface above the Lifshitz transition and finite-range electrostatic impurity scattering. Moreover, Ref. [99] studied the effect of hydrostatic pressure on the resistance minimum and concluded that it arises from

impurity scattering. The impurities were speculated to be oxygen vacancies. A strong pressure and temperature dependence of the STO dielectric constant combined with thermoactivated charge trapping would lead to the resistance [99] minimum. We will address this point extensively in Chapter 6 on LAO/STO doped with $Eu_{1-x}La_xTiO_3$.

1.3. The Anomalous Hall Effect in $SrTiO_3$-based heterostructures

An often used signature of (ferro)magnetism in STO-based interfaces is the Anomalous Hall Effect (AHE). The AHE is a quite complicated and still not fully understood effect, and before reviewing earlier studies of the AHE in the STO-based heterostructures, a general introduction will be given. For a detailed review see Ref. [100].

1.3.1. Mechanisms of the Anomalous Hall Effect and the Ferromagnetic Rashba Model

The AHE is a long-known phenomenon. In ferromagnetic metals there is, besides the ordinary Hall effect, which is due to the Lorentz force and proportional to the applied perpendicular magnetic field, an additional contribution to the Hall voltage, which is proportional to the magnetization [100]. Pugh and Lippert [101, 102] introduced an empirical formula:

$$\rho_{xy} = \rho_{xy}^{OHE} + \rho_{xy}^{AHE} = R_0 H_z + R_S M_z \tag{1.1}$$

R_0 depends on the carrier concentration (in case of one band transport), whereas R_S depends on many parameters of the system, and especially on the longitudinal resistance.

Historically, three main mechanisms have been proposed: skew scattering [103, 104], side jump [105] and an 'intrinsic contribution' or 'anomalous velocity' contribution, suggested very early on by Karplus and Luttinger [106]. In an electric field, electrons acquire an additional amount of group velocity (the anomalous velocity), which is perpendicular to the applied electric field. In non-magnetic materials the sum of the anomalous velocity over all occupied band states is zero, but at certain conditions that is not true for ferromagnets and the AHE appears. It is intrinsic, for clean metals, and nowadays it would be called a Berry phase effect. A different

picture, involving impurities rather than the clean band structure, was proposed by Smit. He proposed that origin of the AHE is an asymmetric scattering from impurities due to the SOI. This scattering is called skew scattering [103, 104]. Berger, finally, proposed a mechanism called side jump: when an electron travels in a solid in the presence of spin-orbit coupled impurities, it will experience electric fields, which will be opposite for approaching and leaving the impurity. The electric fields will produce an electron velocity deflection in opposite directions. Time integration of the velocity deflection then will be the side jump distance.

In modern literature, linear transport theories gained in popularity to study the AHE , because they allow the treatment of the AHE within the same model. These theories are semiclassical Boltzmann transport theory [107, 108] and microscopic theories based on the Kubo formalism [107, 109] and the Keldysh formalism [110, 111]. They produce similar predictions [100, 107, 108]. In such theories, the classification of contributions to the AHE is based on the dependence of the conductance on the Bloch-state transport lifetime τ [100]. In this classification, the skew-scattering term is defined as a term proportional to τ. The underlying reason for the dependence on τ is the fact that the principle of detailed balance in the semiclassical Boltzmann transport has to be abandoned. The principle states the equality between two transition probabilities $W_{n\to m}$ from the state n to m and the opposite one $W_{m\to n}$ [100]. However, this is not correct in the presence of SOC, because the transition probabilities will be different for right- and left-handed transitions with respect to the magnetization direction [100]. To evaluate this through the Boltzmann equation requires solving it using a collision term with properly defined transition probabilities. The presence of asymmetric scattering rates in the collision term leads to two contributions to the AHE. One of them is proportional to τ, and is the skew scattering contribution. The second term is independent of τ, and sometimes called intrinsic skew scattering [108]. This rather confusing term indicates that, like the skew-scattering term, it originates from the collision term, which would correspond to the historical definition of the skew scattering [100, 103]. Still, unlike the skew scattering in the definition through the Bloch-state transport lifetime it is independent of τ. This term was discarded in early semiclassical studies, although being of the same order of magnitude as a side jump [100].

As two contributions to the AHE are defined through the new classification, other contributions are also needed to be redefined. The intrinsic contribution σ_{xy}^{int} can be defined as the dc limit of the interband Hall conductivity. As we mentioned, it depends on the band structure and arises in ferromagnets when the SOI is present. This mechanism is directly related to an electron Berry's phase curvature [112–114] and proportional to the integral of the Berry curvature of each occupied state over the Fermi sea [100]. The side jump contribution emerges from the

displacement of a Gaussian wave packet with an incident wave vector **k**, when that wave packet is scattered from a spherical impurity in the presence of SOI. The displacement is transverse to **k**.

The intrinsic contribution and the side jump contribution are independent of τ. Together with the intrinsic skew scattering, three terms independent of τ are already introduced. However, the effects due to coordinate shifts during scattering events [107, 108, 115] give rise to one more contribution independent of τ. To understand this contribution, let us consider a quasiparticle experiencing scattering from a side jump in the presence of external electric field. Its potential energy will change, but because the total energy is conserved, it will acquire additional kinetic energy [115]. As a result, there is an additional correction to the momentum distribution function because the equilibrium distribution is not stable anymore and has to be compensated by an additional term [115]. That term is named the anomalous distribution and led to the contribution to the AHE called 'the contribution due to the anomalous distribution' [107, 108, 115]. However, for the sake of simplicity, the side jump is often defined as $\sigma_{xy}^{sj} \equiv \sigma_{xy}^{AHE} - \sigma_{xy}^{skew} - \sigma_{xy}^{int}$. In this definition, other contributions, such as the intrinsic skew scattering and the contribution from the anomalous distribution are included in the side jump term despite their different physical origin [100]. In the microscopic theories all these contributions are usually called ladder-diagram vertex corrections to the conductivity.

One of the main advantages of defining the contributions through τ is the possibility to use a scaling law for the AHE analysis. From an experimental point of view, it means that the analysis of the interdependence of σ_{xy}^{AHE} and σ_{xx} can be used to separate the various contributions because $\sigma_{xx} \sim \tau$. Usually, the longitudinal resistance ρ_{xx} and the Hall resistance due to the AHE ρ_{xy}^{AHE} are used for this, connected through the conductivity tensor, which yields the relation $\rho_{xy}^{AHE} \approx \sigma_{xy}/\sigma_{xx}^2 \approx \sigma_{xy}\rho_{xx}^2$ [100]. For various mechanisms, $\rho_{xy}^{AHE} \sim \rho_{xx}^{\beta}$, where β is determined by the mechanism under consideration [100]. In terms of the conductance σ, the skew scattering contribution to the AHE, σ_{xy}^{skew}, is $\sim \tau$, and the scaling relation becomes $\sigma_{xy}^{AHE} \sim \sigma_{xx}$ ($\rho_{xy}^{AHE} \sim \rho_{xx}$) with $\beta = 1$. The contributions independent of τ give a scaling law $\sigma_{xy}^{AHE} \sim \sigma_{xx}^0$ ($\rho_{xy}^{AHE} \sim \rho_{xx}^2$).

A model which gained in popularity in modern literature to study the AHE, is the ferromagnetic two-dimensional Rashba model [11]. There is extensive literature dedicated to this model, see [110, 111, 116–122]. The Hamiltonian for the ferromagnetic Rashba model can be written in the following form ($\hbar = 1$):

$$\hat{H}(\mathbf{p}) = \frac{\mathbf{p}^2}{2m}\hat{1} + \lambda \mathbf{p} \cdot \hat{\sigma} \times \mathbf{e}^z - \Delta_0 \hat{\sigma}_z + \hat{V}(\mathbf{r})\hat{1} \tag{1.2}$$

where **p** is the in-plane momentum, m is the electron mass, $\hat{1}$ is the unitary ma-

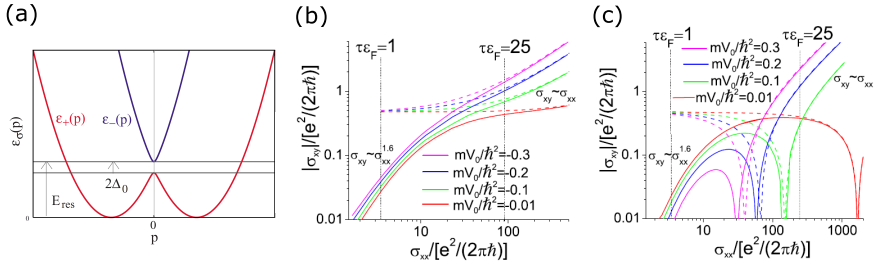

Figure 1.5: (a) The band dispersion described by Eq. 1.3 without the scattering term. The figure is reprinted from Ref. [111]. Copyright 2010 by the American Physical Society. Calculations of the absolute value of the Anomalous Hall conductivity versus the longitudinal conductivity for (b) attractive and (c) repulsive impurity potentials. Note that on the last panel, the AHE changes its sign near the cusps. The figures (b) and (c) are reprinted from Ref. [116]. Copyright 2009 by the American Physical Society

trix, λ is the Rashba SOC constant, $\hat{\sigma} = (\hat{\sigma}^x, \hat{\sigma}^y, \hat{\sigma}^z)$ are Pauli matrices, $\mathbf{e}^z$ is the unit vector in the z direction, δ_0 the mean-field exchange splitting, and $\hat{V}(\mathbf{r}) = V_0\hat{1}\sum_i \delta(\mathbf{r}-\mathbf{r}_i)$ is a δ-scatter impurity potential, where r_i is the position of impurity i. This simple model captures most of the important features such as the intrinsic and the extrinsic contributions as well as taking into account both the majority and minority spin Fermi surfaces. The band dispersion of the Hamiltonian without the last term will be:

$$\varepsilon(\mathbf{p}) = \frac{\mathbf{p}^2}{2m} - \sigma\Delta_{\mathbf{p}} \tag{1.3}$$

$$\Delta_{\mathbf{p}} = \sqrt{\lambda^2\mathbf{p}^2 + \Delta_0^2} \tag{1.4}$$

This dispersion is shown in Fig. 1.5a. As can be seen from the figure, there are three clear regions. The first is when only the majority band is occupied; then all mechanisms will contribute [116, 121, 122]. When the Fermi level lies in the gap, the intrinsic contribution is enhanced. The two bands have Berry curvatures with opposite signs near $\mathbf{p} = 0$, therefore a large intrinsic AHE arises only in the gap region [111, 117, 123]. When both bands are occupied, the skew scattering contribution becomes dominant [110, 111, 116, 119, 120].

A minimal model for the AHE in 3D ferromagnet can also be constructed based on the 2D ferromagnetic Rashba model. In the presence of SOI in a 3D ferromagnet, majority and minority spin Fermi surfaces will avoid touching points for a particular projection of Bloch momentum k_x along a magnetization direction. To account for most of the AHE, one can choose such $\mathbf{k}$ point that the energy gap will be minimum and, therefore, intrinsic contribution will be maximum. When expanding a Hamiltonian around the $\mathbf{k}$ point, it may be possible to obtain an effective Hamiltonian similar to Eq. 1.2. Note that in the Rashba model λ is the SOC con-

stant and Δ_0 is the Zeeman splitting, but in the minimal model λ is the Fermi velocity and Δ_0 is the SOI. Therefore, in the minimal model the SOI opens the gap [100, 111]. Moreover, the Hamiltonian of the minimal model for the general case of a 3D ferromagnet should contain Rashba-like and Dresselhaus-like contributions.

Numerical calculations of σ_{xy}^{AH} based on the Rashba model as well as on the minimal model [111, 116, 123] identified three distinct regimes: a skew scattering dominated regime ($\sigma_{xy}^{AH} \sim \sigma_{xx}$) with a crossover to an intrinsic-dominated regime ($\sigma_{xy}^{AH} \sim const$) with further crossover to an incoherent regime ($\sigma_{xy}^{AH} \sim \sigma_{xx}^{1.6}$) (Fig. 1.5b). The last regime is also referred to as a bad metal regime [100] and associated with $\sigma_{xy}^{AH} \sim \sigma_{xx}^{1.8}$ observed in some experiments. The last regime arises due to influence of finite-lifetime disorder broadening on σ_{xy}^{int}, which is quickly diminished by disorder.

All three regimes have been observed in experiments on various systems. The skew scattering has been reported in Fe doped with Co and Si [124, 125]. The bad metal regime has been identified in anastase and rutile phases of $Co_xTi_{1-x}O_{2-\delta}$ [126], Fe [127], and Fe_3O_4 [128]. The intrinsic mechanism has been reported in diluted magnetic semiconductors such as $Ga_{1-x}Mn_xAs$ [129] and metals Fe, Gd, Co, Ni [130]. However, there are some important limitations to an interpretation of experimental data based on this model. Ref. [116] showed that a change of sign of the impurity potential changes the sign of the skew scattering, and data do not collapse anymore, especially near the intrinsic to extrinsic crossover (Fig. 1.5c). Moreover, a recent study [118] found that the scaling $\sigma_{xy}^{AH} \sim const$ can also arise due to skew scattering involving rare impurities pairs, separated by a distance of order or less than the Fermi wave length [131].

1.3.2. The Anomalous Hall Effect in $SrTiO_3$-based heterostructures

For the systems of interest for this thesis, the AHE was reported in LAO/STO [36, 78, 96], in LAO/ETO/STO [132], in NGO/STO [91], in LAO/$La_{7/8}Sr_{1/8}MnO_3$/STO [133] in $LaAl_{1-x}Mn_xO_3$ (LAMO/STO) [134, 135] and in spinel/STO interfaces such as γ-Al_2O_3/STO, $CoAl_2O_4$ and $NiAl_2O_4$ [78, 136]. Interestingly, the AHE is usually observed when the $d_{xz/yz}$ band is being filled. It corresponds to the two-band regime for most heterostructures, except in case of γ-Al_2O_3/STO, where $d_{xz/yz}$ is lying lower than d_{xy} [78, 137]. Gan *et al.* obtained a rather intriguing result. In their work on LAMO/STO, they found that the AHE in the samples with a doping concentration of x=0.25 showed behavior similar to other STO heterostructures, but starting from x=0.3 the AHE is observed in the one-band regime, which corresponds to only the d_{xy} band filling [134, 135]. The AHE in STO-based structures is usually

not accompanied by *MR* hysteresis [36, 78, 91, 96] except for LAO/ETO/STO, which showed a small amount of hysteresis at very low temperatures [132]. Furthermore, Ref. [138] reported an AHE at the interface between LAO and STO doped by Fe, but in that case the AHE signal was vanishingly small, and this work is not considered further here.

The first model proposed for the AHE in LAO/STO was based on the above mentioned coupling between the $3d_{xz/yz}$ electrons and localized magnetic moments. A problem with the model is that the AHE in these systems is observed in a smaller temperature range than the range with the two band behavior. A possible explanation would be that the system should be below the Kondo temperature, but as discussed in Section 1.2.3 this picture has been seriously challenged. In LAO/ETO/STO, which has been shown to be ferromagnetic [132, 139], the situation seems to be simpler. XMCD measurements revealed the presence of a significant orbital moment of the Ti below the Curie temperature of ETO [132]. Above the Lifshitz transition, the interaction of the orbital moment of the $3d_{xz/yz}$ electrons with such localized magnetic moments can then lead to the AHE through the skew scattering mechanism [132]. As a side note, the method used in Refs. [132] to extract the magnitude of R_{xy}^{AHE} is arguable because it does not take into account any functional dependence of the AHE contribution on magnetization or magnetic field.

A more advanced model to capture the actual contribution of the AHE in presence of the 2-band behavior was proposed by Gunkel *et al.* [91]. Here, the AHE contribution was described by a Langevin-like function (essentially describing the change in polarization of the localised moment; for more details see Chapter 3). In this way, they found a linear dependence of the Anomalous Hall resistance on the longitudinal resistance for samples grown at different pressures and attributed this to skew scattering. Such a description could indicate that magnetic impurities are the main mechanism of magnetism in STO-based interfaces. Simply put, an increase of oxygen pressure should decrease the number of oxygen vacancies. In consequence, a smaller concentration of localized Ti^{3+} moments is expected, and in samples grown at higher pressure the concentration of magnetic moments should be lower. However, the authors of Ref. [91] observed *enhancement* of the AHE in samples grown at higher pressures and, therefore, excluded the oxygen vacancies as a source of magnetism. Instead, they attributed it to an indirect effect of Sr vacancies because high growth pressure leads to an enhanced number of such vacancies. The method of Ref. [91] was also used in a study on LAO/$La_{7/8}Sr_{1/8}MnO_3$/STO [133]. The authors proposed a similar picture to LAO/ETO/STO but instead of Eu^{2+} now Mn^{2+} ions play the role of scattering centers. Surprisingly, the scaling law for the AHE in LAMO/STO indicated an intrinsic mechanism as the dominant contribution to the AHE [134]. The study of

γ - Al_2O_3/STO [78] observed correlations between the ferroelastic domains and the AHE. Finally, besides the above mentioned work, [75] proposed an explanation of the AHE based on electron pairing, but (more) experiments need to be done to confirm this theory.

What is clear at the moment, is that there is no dominant view on the origin of the AHE at oxide interfaces, due to complex entanglement of AHE and Kondo-like behavior, sample variation between experiments, data analysis, and non-trivial results, as well as a somewhat over-emphasized interpretation toward skew-scattering as the only mechanism of AHE in STO-based heterostructures.

1.4. Titanates (RE)TiO_3, where Re=La, Eu and Gd

In the present work, interfaces have been studied involving $LaTiO_3$, or delta doping with $GdTiO_3$, $EuTiO_3$ and $Eu_{1-x}La_xTiO_3$. The (magneto)conductance properties of the interfaces will be considered in the corresponding chapters. Here, a brief overview is given of the growth challenges for titanates, and some bulk, thin film and basic interface properties are given.

LTO, GTO, ETO and ELTO are rare earth titanates ((RE)TiO_3) with the perovskite structure. Most of the research on (RE)TiO_3 films has been done using PLD [139–150] or MBE [151–154] as the growth technique. Growth of stoichiometric (RE)TiO_3 films is challenging due to the sensitivity to the growth conditions. In particular, in an oxygen-rich atmosphere the pyrochlore phase ($Re_2Ti_2O_7$) rather than the perovskite phase tends to form [144, 155]. Furthermore, the absence of a capping layer leads to a replacement of Ti^{3+} by Ti^{4+} in the surface layers [142, 143]. Besides, films grown on STO absorb more oxygen from the substrate, and the amount of Ti^{3+} will decrease [142, 143]. This leads to the occurrence of magnetic dead layers at interfaces and surfaces of (RE)TiO_3 films (RTO) [143, 156]. Such dead layers are paramagnetic because of the presence of Re^{3+} ions [143]. Note that in case of $EuTiO_3$ the picture will be more complicated because Eu can either be 3+ or 2+, and the oxidation process due to STO and oxygen atmosphere occurs differently.

1.4.1. $LaTiO_3$

LTO is an antiferromagnetic Mott insulator, due to the single Ti 3d electron in its trivalent state, with the orthorhombic crystal structure [157]. The antiferromagnetic ordering arises from localized Ti^{3+} moments below the Néel temper-

ature around 140 K [157, 158]. At even lower temperatures spin-canting leads to a small ferromagnetic moment [157] of around 0.45-0.57 μ_B per Ti [159–161]. The LTO/STO (001) interface is another one of the most studied conducting oxide interface system [140, 162]. Ref. [140] considered the picture to be similar to LAO/STO. In that picture conductance is arising because LTO is polar along the (001) crystal direction, and, therefore, charge transfer to the interface will occur. However, other scenarios have also been considered. In this case, the polar discontinuity can be also resolved by a variable valence of Ti at the LTO/STO (001) interface [163, 164]. Ref. [141, 162] argued that strain impose by the STO substrate is able to induce a lattice distortion and this mechanism would make the insulating LTO metallic. In addition, LTO is sensitive to chemical off-stoichiometry: La/Sr intermixing [157, 165–167], or oxygen and lanthanum off-stoichiometry [168] can transform LTO into a conducting state. Similar to LAO/STO (001) this system exhibits superconductivity [140, 169], two-band behavior [59] and shows signatures of WAL [170].

1.4.2. $GdTiO_3$

GTO is a ferrimagnetic Mott insulator with Curie temperature of 32 K [157, 171]. The magnetic moment from the seven $4f$ electrons of the Gd atom are coupled antiferromagneticaly to the magnetic moment of the one $3d$ electron of the Ti atom. The saturation magnetization is 6 μ_B per Ti [157], but in films much smaller values have been reported. GTO shows absence of hysteresis in films [144, 154, 156, 172] and bulk [157]. GTO is polar along (001) the direction like LTO and LAO and the interface between GTO and STO hosts a 2DEL [173, 174]. Similar to LTO, other mechanisms than the polar discontinuity can again be a reason for interface conductivity. So far there was no demonstration of the AHE in this system, although hysteretic and anisotropic magnetoresistance indicate the presence of magnetism in the 2DEL [173, 174].

1.4.3. $EuTiO_3$ and $Eu_{1-x}La_xTiO_3$

ETO stands out in the RTO family. Unlike the rest of Re atoms, the most common oxidation state of Eu is Eu^{2+}. Therefore, the Ti atom is in a tetravalent state in ETO and does not contribute to the magnetization. Also, ETO, like STO, is a band insulator. It also is an antiferromagnet with a Néel temperature around 5.4 K [175–181]. ETO is often considered to be cubic down to low temperatures. However, there is a debate about the presence of a cubic to tetragonal transition. Ref. [177, 178, 180,

182, 183] reported such a transition around 282 K, while Ref. [184, 185] observed a lower transition temperatures. On the other hand, the authors of [179] did not confirm the occurrence of a transition. The result was also challenged by further work of Ref. [186], who argued that, due to a small change in the ratio between the in-plane and out-of-plane lattice constants, advanced techniques are required to detect the structural transition in ETO. Another intriguing property of ETO is the coupling between the spin lattice and an infrared-active phonon in ETO [181, 187], which allows transforming the antiferromagnetic and paraelectric state into a ferromagnetic and ferroelectric one by stress [153, 187]. Moreover, the magnetic state in compressively strained ETO can be controlled by electric fields [187, 188].

ETO is not polar along (001) direction. Therefore, it cannot be used to create a 2DEL at the interface with STO by means of the polar catastrophe. Stoichiometric ETO grown on STO should be in the antiferromagnetic state because ETO is almost isostructural with STO [152]. Indeed bulk-like behavior was reported for films grown by MBE [152] and for post-annealed PLD films [147, 148]. At the same time, non-annealed films grown by PLD showed ferromagnetic behavior [147, 148, 189], which was attributed to the formation of oxygen vacancies [147] and a longer out-of-plane lattice constant [148]. Moreover, amorphous ETO also showed ferromagnetism [190]. It is possible to use ETO to delta dope LAO/STO in order to induce magnetism [132, 139]. The ETO magnetic state in these films was identified as ferromagneticaly ordered below 8 K [132, 139]. Kondo-like behavior [132, 139], WAL [191], superconductivity and gate-tunable AHE [132] have all been reported for the films.

$Eu_{1-x}La_xTiO_3$ or ELTO has different properties from ETO. Ref. [192] found that doping of bulk ETO with 10 % La introduces electrons into the conduction band of the $3d$ t_{2g} states and makes ETO a ferromagnetic metal with Curie temperature of 8 K. Further research on thin films confirmed that even 1% of La doping is enough to make ELTO conducting [145]. This compound exhibits negative *MR* indicating the exchange coupling between itinerant electrons of Ti and localized spins of Eu [192]. Note that such mechanism is distinct from GTO, where the Ti electrons are localized [192].

Ferromagnetism has also been reported in the films, but remanent magnetization was absent [145, 151]. Such behavior was explained by a change of the magnetic order from antiferromagnetic in zero field to ferromagnetic in high field [151]. Moreover, the AHE has been observed in the films prepared on LSAT substrate [145, 151]. The AHE exhibits a sign change and a dependence on the carrier concentration [145]. Authors of [145] considered it as indications of the intrinsic origin of the AHE due to the band structure, which also was supported by theoretical calculations. Indeed, correlation between the sign change of the intrinsic AHE and the

band crossing points was declared [145]. These band crossings are crossings between d_{xy} and $d_{xz/yz}$ bands, which are split due to tetragonal distortions in the films grown on LSAT [145, 151]. Intriguingly, in the films grown by MBE and in some films grown by PLD non-monotonic magnetic field dependence of the AHE has been observed [151]. Furthermore, this effect was present in oxygen deficient ETO films [151]. The authors of [193, 194], who studied Sm doped ETO films on LSAT, attributed non-monotonic behavior to an additional contribution of topological AHE. But authors of [151] argued that this behavior is due to a change of Zeeman splitting during a magnetization process.